PAPER

A measure of fast ion beta at marginal stability in the reversed field pinch

To cite this article: W. Capecchi *et al* 2019 *Nucl. Fusion* **59** 086026

IOP Publishing | International Atomic Energy Agency Nuclear Fusion

Nucl. Fusion **59** (2019) 086026 (10pp) https://doi.org/10.1088/1741-4326/ab2473

A measure of fast ion beta at marginal stability in the reversed field pinch

W. Capecchi[1], J.K. Anderson[1], P.J. Bonofiglo[1], J. Kim[1], R.M. Magee[2], K.J. McCollam[1], R. McConnell[1], E. Parke[2] and J.S. Sarff[1]

[1] Department of Physics, University of Wisconsin, Madison WI, United States of America
[2] TAE Technologies, Foothill Ranch CA, United States of America

E-mail: william.capecchi@gmail.com

Received 11 January 2019, revised 21 April 2019
Accepted for publication 24 May 2019
Published 27 June 2019

Abstract

Energetic ions are well confined in the core of the reversed field pinch and a substantial population develops rapidly during tangential neutral beam injection. A saturated fast ion density is observed within several milliseconds and coincides with the onset of energetic particle mode activity. First measurements of the fusion product profile determine the fast ion density and pressure profiles, the latter of which when combined with neutral particle analysis of the energy distribution. These are key measurements in explaining the limiting behavior of the fast ion profile in response to a combination of effects. Tearing mode activity affects the fast ion profile, and the fast ions noticeably influence the core-most tearing mode. The nonlinear situation settles into a marginally stable state where the EPM transports fast ions down a steep gradient to a region where their confinement is limited by stochastic orbit and charge exchange losses. In the state at marginal stability (achieved in one set of experimental conditions with full 1 MW neutral beam power), a critical fast ion beta gradient is measured that limits the core $\beta_f(0) \sim 7.5\%$, or nearly four times the core thermal β, but less than a strictly classical calculation predicts.

Keywords: neutral beam injection, energetic particle mode, critical fast ion beta, reversed field pinch

(Some figures may appear in colour only in the online journal)

1. Introduction

The behavior and confinement of high energy particles is an important aspect of any magnetic confinement fusion reactor concept, as charged fusion products must be confined long enough to transfer their energy back to the plasma to sustain 'burning' conditions. It is well demonstrated that fast ions in a tokamak plasma (born from fusion reactions, ion cyclotron radio frequency (ICRF) heating, or neutral beam injection (NBI)) are generally well confined and thermalize via classical Coulomb collisions. A sufficiently intense fast ion population (particularly when super-Alfvénic), however, can excite collective instabilities that can lead to resonant fast ion transport [1].

These fast ion driven modes fall into two categories. Alfvén eigenmodes (AEs) are weakly damped normal modes of the plasma, characterized by a gap in the shear Alfvén continuum due to a periodicity in the Alfvén speed related to toroidicity, ellipticity, etc. The energetic particle mode (EPM) is a strongly driven, strongly damped perturbation with frequency near the Alfvén continuum, appearing when the fast ion pressure is comparable to the thermal plasma pressure and continuum damping is exceeded. The EPM is theoretically approached by considering the energetic ion component at negligible density but pressure comparable to the thermal plasma (treated as a magnetohydrodynamic fluid) [2]. The stability is often characterized as a balance between a $\nabla\beta_f$ drive term and continuum damping [3, 4] where β_f is the local ratio of fast ion pressure to magnetic field pressure.

In the experiments reported here for reversed field pinch (RFP) plasmas, the onset of EPM limits the fast ion pressure. There is an absence of significant AE activity that has been observed in other toroidal plasmas to correlate with limiting the fast ion pressure. The observed behavior for these RFP plasmas

therefore illustrates the case where the fast ion pressure must be sufficiently large so as to excite strongly damped modes. Consistent with this, the measured fast ion beta is relatively large. Consider seminal energetic particle physics studies in the DIII-D tokamak, utilizing a large range of magnetic field, shaping and current profiles, and high power NBI. Toroidicity-induced Alfvén eigenmodes (TAEs) were first identified in DIII-D in L-mode limiter discharges at a $\beta_f \sim 1\%$ [5], roughly half the value predicted by a strictly classical calculation [6]. Techniques to increase the damping, and hence stability, of the TAE were identified, including increased thermal plasma pressure (β_{thermal}) and advanced shaping. At $\beta_N \sim 3.5$ (where $\beta_N \equiv \beta_t a B_t / I_p$ and β_t is the thermal toroidal beta) the TAE was suppressed, but instead the beta-induced eigenmode (BAE) appeared at around half of the TAE frequency. This frequency gap is caused by a compressional response of the plasma to shear Alfvén waves in the presence of finite pressure and curvature [7]. In a more stable double null divertor discharge at high magnetic field and low density, strong NBI excited a chirping EPM which limited the fast ion beta near $\sim$1%, but with fast ion speed below the Alfvén speed [8]. Work in engineering of the equilibrium magnetic profiles to further improve fast ion confinement is ongoing [9].

The RFP presents a complementary environment for study of fast ion driven instabilities, with a relatively weak but strongly sheared magnetic field that generates an Alfvén continuum distinct from that in a tokamak or stellarator. Nearly all the confining field (including the toroidal component) is generated by current within the plasma and the modulus of the magnetic field takes on a unique shape: the field is strongest at the magnetic axis and the poloidal component is dominant beyond mid-radius. The absence of a high field side in the RFP places ∇B in the minor radial direction, and the curvature is dominated by the poloidal field except in the immediate vicinity of the plasma core. The resulting guiding center drift velocity is therefore perpendicular to both minor radius and local B on a magnetic surface. Drifts across surfaces are very small and the banana width for trapped orbits is smaller than the fast ion Larmor radius ($\rho_{\text{L,fi}}$).

The RFP's magnetic safety factor profile $q = \left\langle \frac{rB_\phi}{RB_\theta} \right\rangle$ (see examples in figure 2) is strongly sheared, implying strong damping of modes in the Alfvén continuum. The low value of q permits many rational surfaces where long wavelength $m = 1$, $n \geqslant 5$ tearing modes are resonant. The overlap of magnetic islands leads to thermal confinement in the standard RFP that is governed by Rechester–Rosenbluth-like stochastic transport [10]. Despite the RFP's weak toroidal field and multiple resonant tearing modes which could diminish fast ion confinement [11, 12], NBI-born fast ions in low concentration are observed to slow classically and have a confinement time much larger than thermal particles. The notable lack of radial transport within the modestly stochastic magnetic field is understood to result from the decoupling of the fast ion orbits from the magnetic perturbations. Core-born NBI ions traveling in the direction of plasma current are routinely confined for up to a classical slowing time [13] of about 20 ms in the plasma studied herein. At mid radius, the effect is lessened as global tearing modes with the proper poloidal and toroidal mode numbers can affect the ion orbits [14] resulting in overlapping ion guiding center islands and stochastic orbits. More recently, core fast ion confinement degradation due to symmetry breaking by the core-most tearing mode was reported [15, 16].

In this work, measurements of the fusion neutron flux and magnetic fluctuations in the Madison Symmetric Torus (MST) [17] help answer the question of what limits the fast ion content in the core of the NBI-heated RFP. Near-classical behavior is initially observed at NBI turn-on as the fast ion population builds. An interesting, stabilizing effect on the core-most tearing mode [18] leads to a transient nonlinear dynamic between tearing mode amplitude and fast ion population during the rapid increase of fast ion content. A saturated fast ion content is observed in the global fusion neutron flux at the onset of EPM activity (with coherent toroidal mode number $n = 5$) after several milliseconds of intense deuterium NBI. While multiple types of magnetic activity are driven by NBI in MST, previous work clearly identifies the bursting $n = 5$ modes as a spatial gradient-driven EPM [19, 20]. The EPM taps free energy from the spatial gradient and transports resonant fast ions outward into a region of higher loss.

The primary result herein is a measurement of the β_f profile in MST with beam energy $E_b = 25$ kV and central magnetic field strength $|B|(0) \sim 0.3$ T and plasma current $I_p = 300$ kA. These conditions most closely match normalized fast ion parameters of fusion alphas in an envisioned RFP reactor [21] with $v_f/v_{th} \gtrsim 10$, $v_f/v_A > 1$ and $\rho_{\text{L,fi}}/a \sim 0.1$. In this case, the core-most tearing mode amplitude is noticeably influenced by fast ion pressure and a quasi-stationary state at marginal EPM stability is observed after approximately one classical slowing time. The effect of the primary tearing modes play a role in determining the total developed fast ion population, which saturates coincident with the onset of EPM activity. The analysis is repeated at higher $|B|(0) \sim 0.5$ T and $I_p = 500$ kA but still with the experimentally maximum $E_b = 25$ kV. The fast ion effect on the tearing instability is much weaker in the higher field, higher plasma current case, and additional caveats muddle a direct comparison of the β_f limit observed in the two cases and are discussed below. This paper is is organized as follows. In section 2, the target plasma conditions and experimental techniques are described. The equilibrium fields and pertinent details of fast ion orbital motion that dictate confinement in the RFP are illustrated. Evidence of a saturated fast ion content is presented through a beam power scan. A description of the fast ion density profile measurement through spatially-resolved counting of D–D fusion neutrons is in section 3. The fast ion pressure profile is shown in section 4 for the two distinct plasma conditions of $I_p \sim 300$ and 500 kA. Section 5 is a discussion of the primary results, including the fast ion excitation of the energetic particle mode by resonant orbits, a clear observation of a subtle nonlinear interaction between the fast ions and the core-most tearing mode, and identification of a critical fast ion beta gradient in a marginally stable state. Concluding remarks follow.

2. Experimental methodology

Figure 1 is a summary of the equilibria of the two sets of discharges studied herein ($I_p = 300$ kA and 500 kA) with plasma current waveforms and timing of the NBI power application shown in (*a*). Panels (*b*) and (*c*) are spectrograms of the n = 5 magnetic activity in a representative discharge from each set. The strong, persisting mode at low frequency is the tearing mode, whose measured frequency is a proxy for the plasma rotation. Alfvénic modes ($f = 50$–200 kHz) observed during NBI ($t = 12$–33 ms) propagate in the plasma frame and in subsequent analyses the plasma rotation is subtracted as a Doppler shift. No significant power is observed above 200 kHz in these experiments. Panel (*d*) is a plot of the spatially averaged toroidal magnetic field (from a toroidal flux measurement), highlighting that the field strength is directly related to the plasma current as a function of time in the RFP, and representative fusion neutron flux (measured by averaging many similar discharges) in each case. Experiments are conducted for a $q(a) = 0$ equilibrium, which is easily achieved through a boundary condition of zero applied toroidal field. The dynamics described here are similar to those in typical reversed toroidal field cases, but the avoidance of multivalued toroidal flux facilitates the use of codes developed for tokamak plasmas. Equilibrium analysis is focused near the end of the NBI pulse at $t = 30$ ms to allow a quasi-stationary state to develop; reconstructed field profiles are plotted in figure 1(*e*). In each case, the electron density is held near 1.0×10^{19} m^{-3} and 0.8 MW of deuterium NBI at 25 kV is injected, with $\frac{v_{beam}}{v_A(0)} \sim 1.25$ in 300 kA discharges and ~0.75 in 500 kA discharges. While not measured directly in these experiments, calculations using typical values of $Z_{eff} = 2$–5 do not change the assessment of sub- versus super- Alfvénic speed of the beam ions. The corresponding Alfvén continuum for the observed modes ($n = 5$ and $m = 0, 1$) is plotted in figure 1(*f*). A toroidicity-induced gap can be seen at $f > 200$ kHz, whereas the core-localized fast ions tend to drive EPM activity at $f < 120$ kHz.

The q profile for each discharge is plotted in figure 2(*a*), along with the analogous fast ion guiding center q, $q_{igc} = q_f = \frac{rv_{\phi,gc}}{Rv_{\theta,gc}}$, the effective motion of the ion guiding center. Note the deviation from magnetic q is reduced at higher current, where the 25 kV D + drifts are reduced proportionally to magnetic field strength. Figure 2(*b*) illustrates the guiding center drift from the magnetic field line due to ∇B and curvature

$$\vec{v}_d = \frac{m}{2eB}\left(v_\perp^2 \frac{\vec{B} \times \nabla B}{B^2} + 2v_{||}^2 \frac{\vec{R_c} \times \vec{B}}{R_c^2 B}\right) \quad (1)$$

where the common approximation to combine the two drifts as a multiplier of ∇B is not allowed due to strong current in the plasma. The in-surface drift decouples fast ion motion on a given flux surface from the dominant local radial magnetic field perturbations, resulting in fast ion confinement well above thermal levels in the RFP.

The resonant locations of multiple low order tearing modes are plotted on the q profiles as are the widths of fast ion guiding center islands. These are set by the radial velocity perturbation at the rational surface in the q_f profile which are related to the magnetic perturbation of the same helicity evaluated at the ion guiding center rational surface. The substantial distance from the magnetic resonance leads to smaller perturbation and resulting island width.

The result for co-injected fast ions is that q_f is shifted upward from q leading to an outward shift of the resonant surfaces identified in the q profile. For sufficiently fast ions, this also makes the core-most $m = 1$ fast ion rational surface correspond to $n = 4$: a helicity without a corresponding resonant magnetic perturbation within the plasma. There is also a substantial radial domain in the core free of ion guiding center resonances. These features make core localized fast ions insensitive to the stochastic magnetic transport, rendering them nearly classically confined, although evidence of a residual effect of the $n = 5$ tearing mode on fast ion confinement has been observed [15]. As the fast ions slow, $\Delta q = q_f - q$ decreases and fast ion island widths increase and begin to overlap causing the particle orbits to become radially stochastic. A similar stochastic orbit occurs for ions at large enough minor radius to be influenced by multiple overlapping islands, even at full energy.

In practice, the high intensity NBI quickly excites high frequency magnetic activity and a saturated fast ion density is observed. Figure 3 illustrates the limiting behavior by plotting the edge-measured magnetic activity and global D–D fusion neutron rate as a function of injected beam power. The beam energy is maintained at 25 kV while the current is operated at three distinct levels shown in panel (*a*). On an individual discharge, the magnetic activity appears as repetitive, discrete bursts of about 150 μs with approximately 500 μs separation between events at full beam power (as plotted in figures 1(*b*) and (*c*). The continuous-looking plot in figure 3(*b*) is a result of averaging many discharges to improve counting statistics of neutron emission. Considerably stronger tearing mode activity at $f < 30$ kHz is excluded from the plots and the plasma rotation is removed such that the frequency axis is in the plasma frame. The total amplitude of the EPM is overplotted with $\lesssim 1$ G for the $I_{beam} = 40$ A case, and reducing step-wise to a faint signal only in the $I_{beam} = 20$ A case. The TRANSP/NUBEAM [22] code computes the classical behavior for NBI in MST [23]; the expected global neutron flux for a 40 A deuterium beam into the MST plasma is included in figure 3(*c*). The TRANSP calculation and the 40 A experimental result show good agreement prior to excitation of high frequency mode activity. At the onset of EPM activity, the measured fusion rate abruptly stops increasing and remains on a saturated level for the remainder of the NBI pulse. Similar results occur for all values of beam current: the fusion rate grows until the onset of EPMs and remains clamped thereafter. However, for the reduced beam current cases, the saturated state is reached with both a longer source time required to excite EPMs and a lower total fast ion content. The latter point is addressed in detail in section 5.

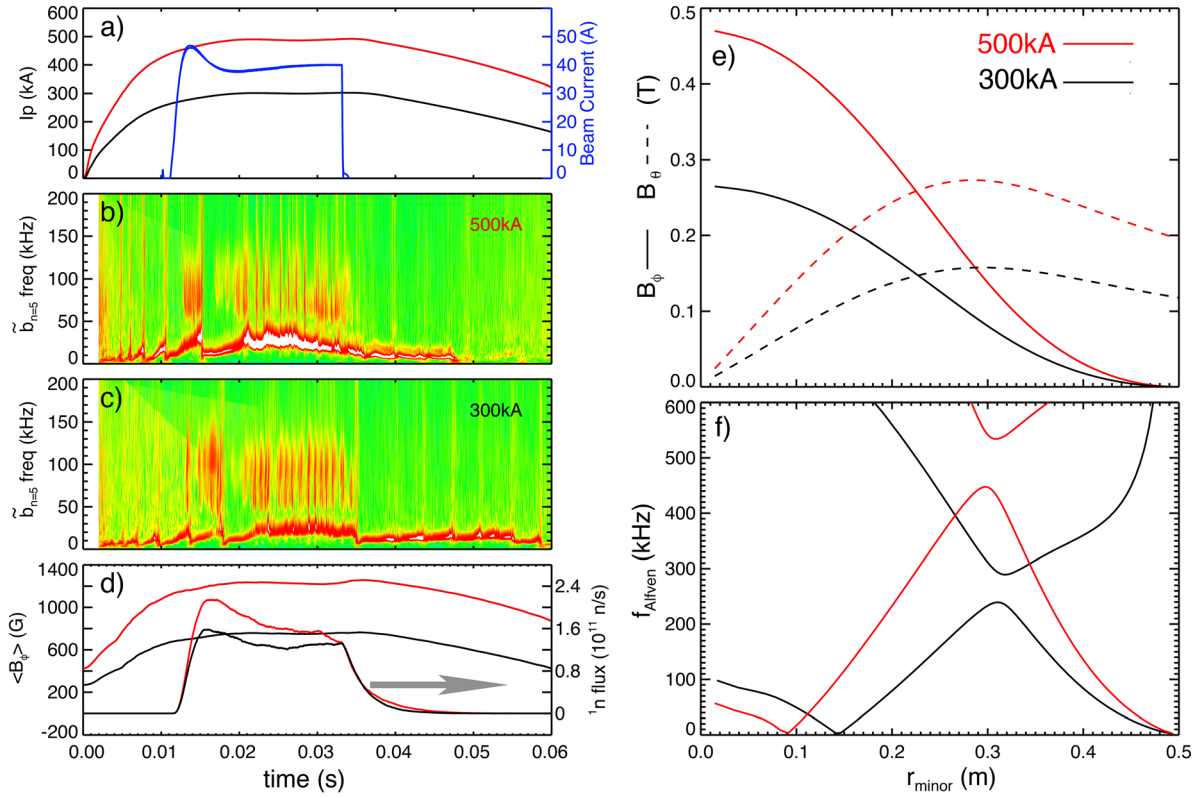

Figure 1. (*a*) Plasma current and timing of NBI heating; (*b*) and (*c*) $n = 5$ magnetic activity in example discharges of 500 kA and 300 kA, and (*d*) toroidal magnetic field strength, where the area-averaged value measured through toroidal flux follows the plasma current and the typical (by averaging many similar discharges) neutron flux measured for each case. (*e*) Typical magnetic field profiles from equilibrium reconstruction at $t = 30$ ms and (*f*) corresponding Alfvén continuum for $n = 5$ perturbations.

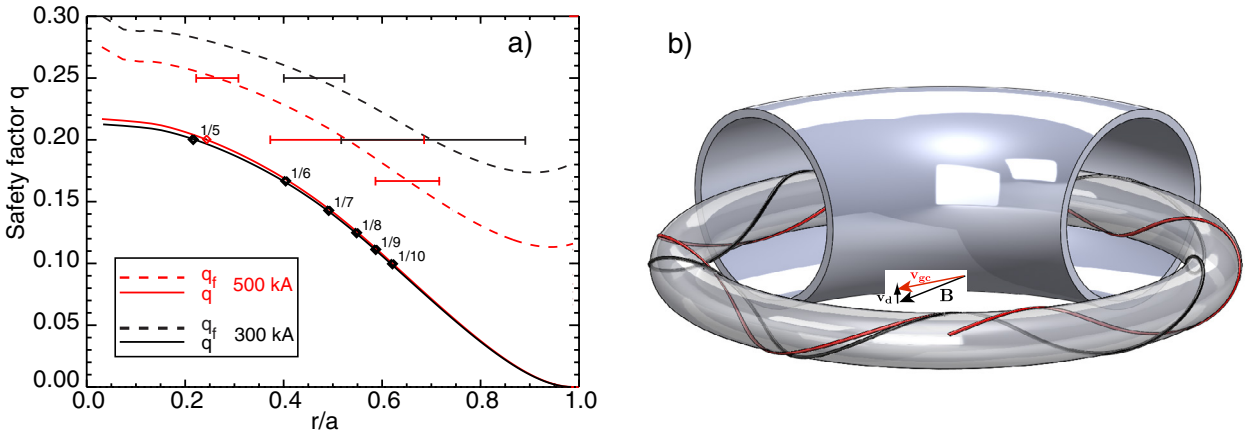

Figure 2. (*a*) Similar safety factor profiles are reconstructed for the two plasma currents, but the fast ion q_f varies substantially from lower to higher B case for 25 kV deuterium injection. The locations of low order tearing mode resonances are plotted on the q profiles, while locations for resonant radial perturbations in guiding center motion are shown on the q_f lines. (*b*) Illustration of the in-surface nature of fast ion guiding center drifts in the RFP geometry.

3. Fast ion density profile measurement

The fast-ion profile in MST is measured through fusion neutron detection, with beam-target fusion the dominant source; thermonuclear flux is negligible since $T_i \leqslant 1$ keV in these plasmas. The fast-ion density n_f is proportional to fusion neutron flux Γ through

$$\Gamma \simeq \frac{1}{2} \int f_f(E) n_i \sigma v \, \mathrm{d}E \, \mathrm{d}V \qquad (2)$$

where $\int f_f(E) \, \mathrm{d}E = n_f$ and the fusion reactivity σv is evaluated using a classically- calculated slowing distribution which has been verified in experiment by neutral particle analysis [24, 25]. The factor of 1/2 is due to the nearly equal branches of the D–D fusion reaction. A suite of absolutely calibrated neutron detectors measure the global flux, and a collimated neutron detector (CiNDe) [26] measures chord-integrated neutron flux by viewing the plasma through a long open bore through neutron shielding material shown in figures 4(*a*)–(*c*).

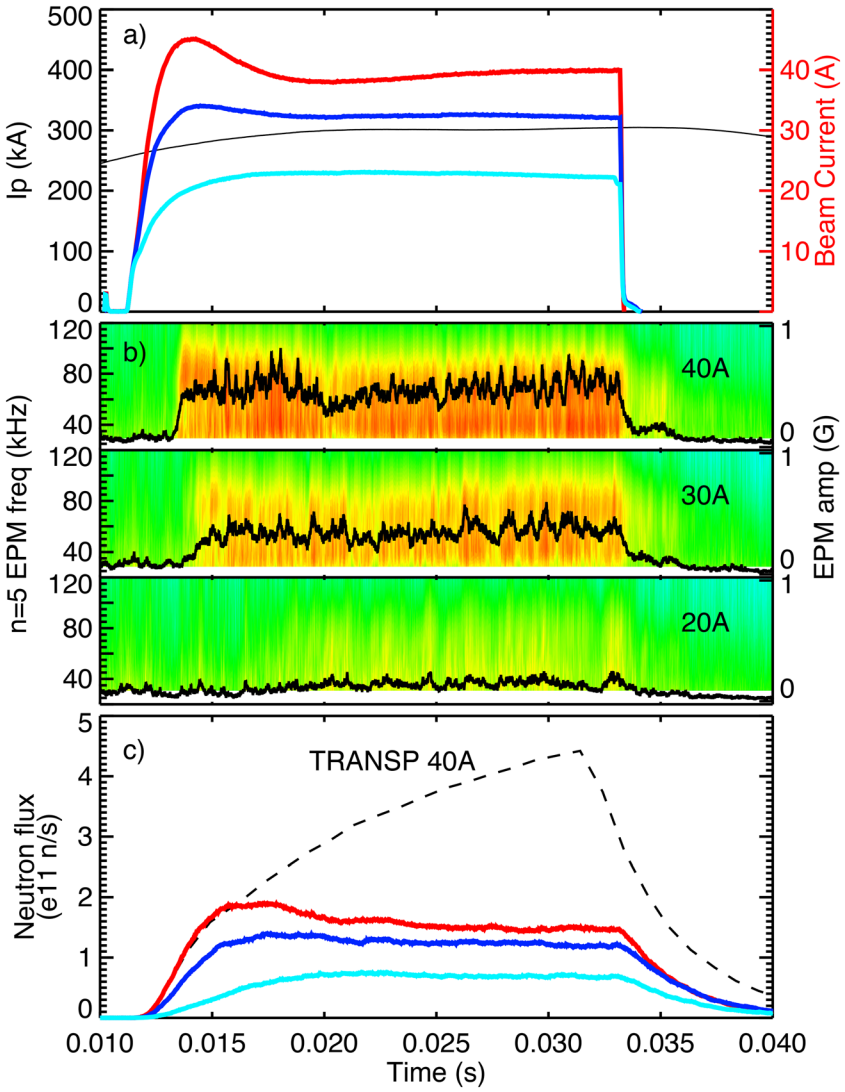

Figure 3. A scan of beam current in deuterium NBI exposes saturated fast ion content. Beam currents of 40, 30, and 20 A NBI into 300 kA plasmas (*a*) result in $n = 5$ EPM activity, with mode onset delayed and amplitude reduced at lower beam power (*b*). The spectrogram shows power in roughly the same frequency band for each case, but the total frequency-integrated amplitude is reduced in each step. After onset of EPM activity neutron flux saturates (*c*), breaking with TRANSP predictions (dashed line) at full beam current, and settling into distinct values for each case.

Fusion neutrons pass with high likelihood directly through the aluminum vacuum vessel and interact with a long, small diameter liquid crystal scintillator.

Although a large amount of polyethylene and lead shielding protect the detector from untoward neutron and gamma radiation, a large background persists. The pollutant signal is quantified by plugging the bore with a solid polyethylene cylinder to block the line-of-sight neutron flux. Differencing techniques between large datasets of plasma-viewing and bore-plugged background cases give a four or five chord profile measurement with tolerable uncertainty, as sketched in figures 4(*d*) and (*e*). Exploiting the fact that the D–D fusion reaction has two equally likely branches, a complementary measure of the fusion product profile was performed by counting 3 MeV protons which promptly escape the confining magnetic field in MST. While a slightly different inversion technique is required due to the curved trajectory, the two techniques agree quantitatively on the fast density profile [27].

The integrated data are inverted using a least squares fit to a two parameter profile and a scale factor is applied to match the absolutely calibrated global neutron measurements [25]. The fast ion energy distribution is incorporated to compute pressure, and equilibrium reconstruction gives magnetic field profiles for a computation of fast ion beta, β_f. In using the fusion neutron flux to estimate the total fast ion population, we assume that the bursting EPM is spatial-gradient driven and does not substantially alter the velocity distribution away from that of classical slowing. While the available diagnostic suite is not adequate for a full fast time-resolved analysis of the distribution, work in [19, 20] and herein can be explained through spatial gradient flattening alone. Foundational literature on EPM stability [3, 4] considers gradients in fast ion beta as the source of free energy; in the NBI-heated RFP, the magnetic field scale-length is much larger than that of the fast ion pressure and the fast ion energy distribution is nearly

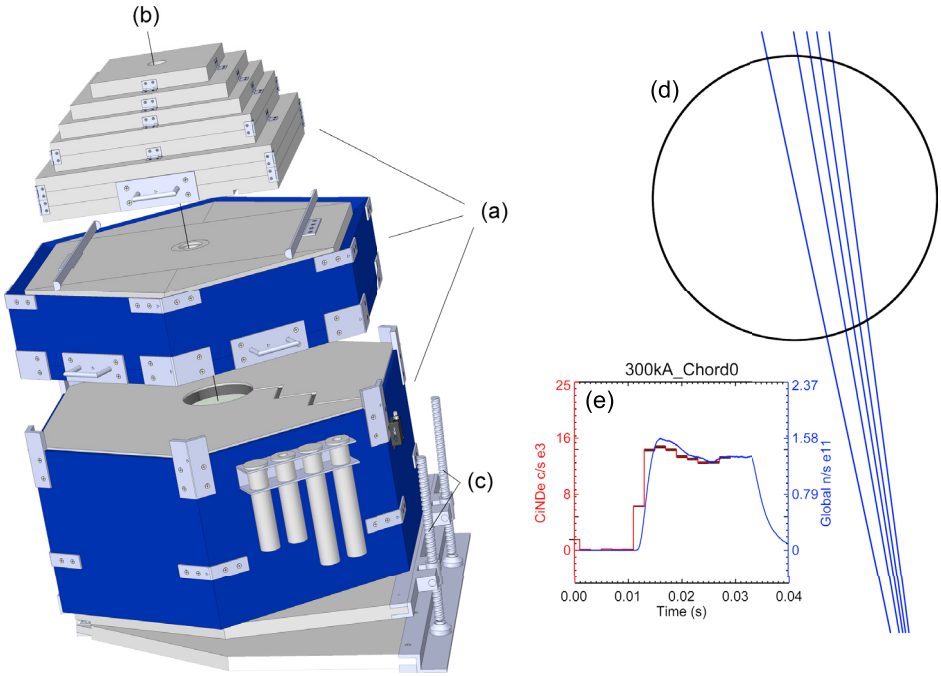

Figure 4. CAD model of collimated neutron detector (CiNDe) constructed in three detachable stages (*a*). The scintillator is placed at the bottom of a bore hole that is 5.1 cm diameter and 92 cm long (*b*) that defines the plasma viewing volume. This is scanned across the poloidal cross section of the machine by adjusting the inclination of the baseplate using a dual worm-screw jack system (*c*). Each of the viewing geometries (*d*) result in raw chord data similar to the example in (*e*). The measured CiNDe count rate (the low time-resolution, red curve and axis in (*e*)) is proportional to global flux (blue curve and axis); in this example through $t = 30$ ms.

constant in radius, indicating that (to within scale factors) $\nabla\beta_f \approx \nabla P_f \approx \nabla n_f$ [25].

4. Fast ion beta at marginal stability

A combination of EPM and tearing activity act to limit the total fast particle content in the RFP; the stabilizing influence of fast ions on the primary tearing mode and the MHD equilibrium [28] creates an interesting nonlinear problem. The critical β_f for destabilizing the EPM is investigated in a large ensemble of 300 kA discharges through a process illustrated in figure 5. The EPM, (*a*), and tearing, (*b*), activity show several interesting features as a function of time. Early in the NBI pulse, there is a dynamic burst of EPM activity while the tearing mode (plotted here as normalized to edge field strength) quickly responds to the fast ion effects. The change in tearing, in turn, has an effect on the fast ion behavior. The notable change in frequency of the upper band of EPM is evidence of the nonlinear problem. Late in time, the situation has evolved to a quasi-stationary state at marginal stability to the EPM. There are two distinct frequency bands of EPM activity, consistent with mode splitting previously observed [29]. Inspection of the Alfvén continuum in figure 1(*f*) suggests the modes are excited near $r \sim 0.1$ m when the strong β_f gradient matches the radius where the continuum crosses $f = 40$–70 kHz.

Fusion neutron flux (time-averaged during the quasi-stationary period) is measured along five viewing chords (*c*), and the fast ion density is reconstructed in (*d*) with a central value approaching 10% of the bulk density. Calculations using the fast particle energy distribution, fusion reactivity cross sections, and equilibrium magnetic field profiles then yield a β_f profile plotted in figure 6, for a single equilibrium condition of $I_p = 300$ kA, at $t = 30$ ms and with full beam power ($I_{beam} = 40$ A) resulting in a central value of $\beta_f(0) = 7.5\%$ exceeding the thermal β by about a factor of four.

Similar experiments performed in 500 kA discharges are shown in figure 7 but the results can not be directly compared to the 300 kA case to infer a strict β_f limit. The effect of the same-energy fast ions (at the experimentally available maximum) in a 5/3 stronger magnetic field lead to reduced effects on the equilibrium and render the fast ions sub-Alfvénic. The effective q_f is not separated as dramatically from magnetic q, and the fast ion effect on core tearing is substantially muted. Tearing activity plays a more important role in limiting the fast ion content in this case though we deliberately avoid the helical state that can spontaneously occur in this plasma current range and dramatically alter fast ion confinement properties in the RFP [16]. The magnetic shear remains virtually unchanged, but, as seen in figure 1(*f*), the slope of the Alfvén continuum scales with magnetic field strength, resulting in stronger continuum damping of the EPM. Nonetheless, the EPM does not require a super-Alfvénic speed for excitation, and they are indeed destabilized and plotted in figure 7(*a*).

The normalized tearing mode amplitude, figure 7(*b*), responds slightly at the onset of the NBI pulse but sinks below 0.5% for only a short period. There is a natural tendency for the tearing mode to grow (on average) with time in these discharges, and the ability of the fast ions to enhance stability until beam turn-off in the 300 kA case is not duplicated in

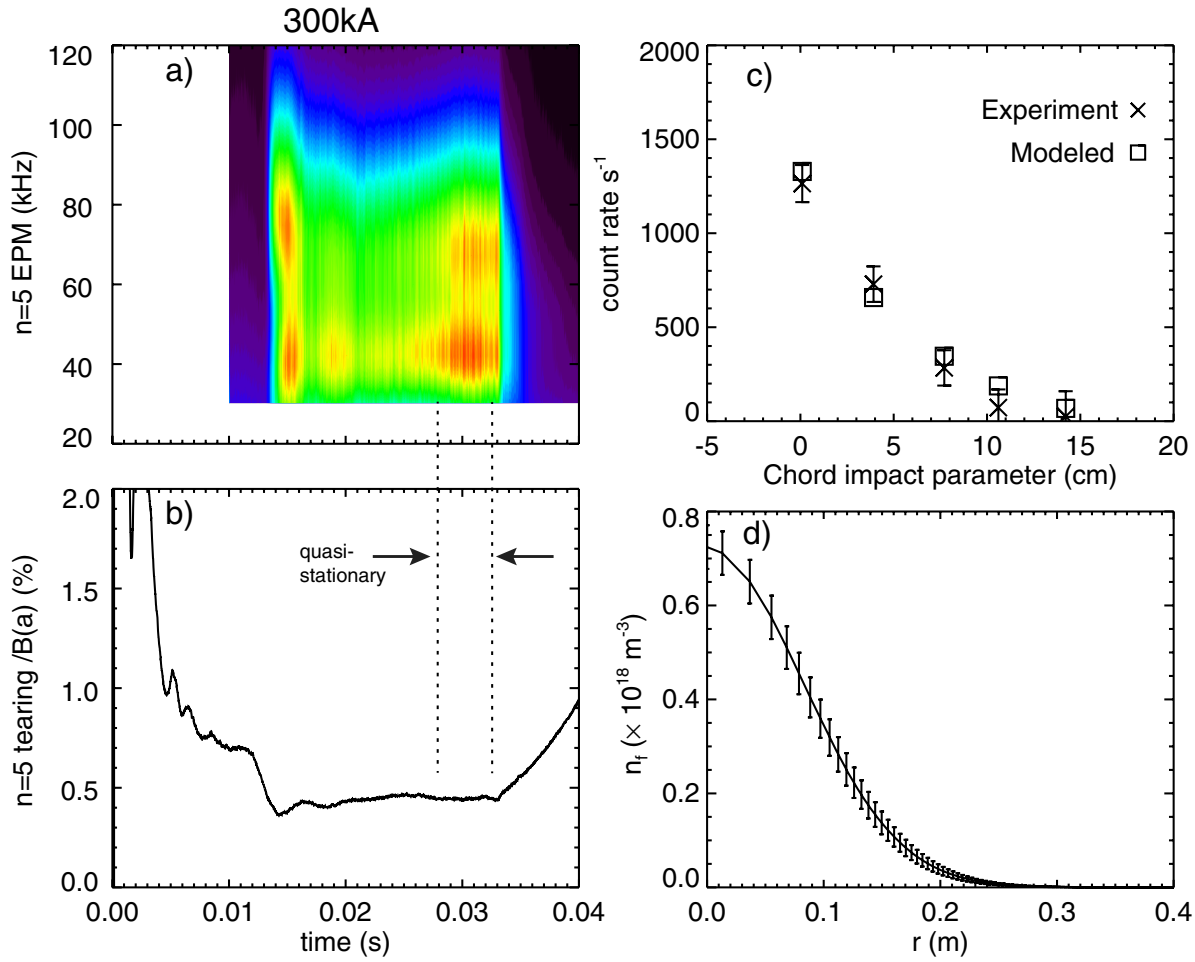

Figure 5. EPM (*a*) and tearing (*b*) activity during D NBI into $I_p = 300$ kA discharges. The fast ion profile is studied at $t = 30$ ms through the chord integrated data and reconstructed fit (*c*) which yield a best-fit fast ion density shown in (*d*).

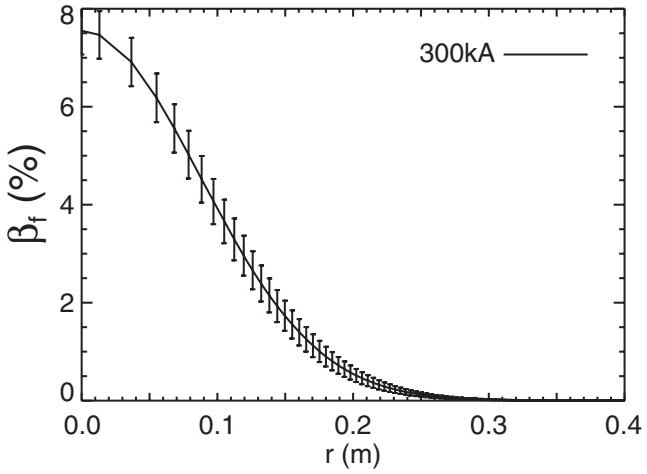

Figure 6. Fast ion beta profile β_f in a quasi-stationary state of marginal stability, measured in the single equilibrium condition of $I_p = 300$ kA, at $t = 30$ ms and with full beam power $I_{beam} = 40$ A.

this experiment. Fusion neutron flux along several chords figure 7(*c*) is used to measure the fast ion density figure 7(*d*) around $t = 30$ ms. The fast ion density is broader and has a lower central value than that in the 300 kA case which is expected due to the stronger remaining tearing activity, discussed below. Both cases show a core-localized fast ion density profile, as the transport and loss at mid-radius steps up due to stochastic fast ion orbits and increased charge-exchange due to higher neutral density.

5. Discussion

Consider again the beam current scan in 300 kA discharges with beam and plasma current, neutron flux, and tearing mode activity plotted in figures 8(*a*)–(*c*). The saturated fusion rate coinciding with EPM activity varies with neutral beam current, indicating a finite (as opposed to immediate) loss in the source/sink balance problem. To clarify, previous work on MST using a hydrogen fueled NBI and diagnosed by neutral particle analyzers hypothesized that EPM activity begins when a critical fast ion population threshold is reached; thereafter a predator/prey relationship emerges where magnetic perturbations transport the entirety of the incoming fast ions [18]. The observed strength and time to onset of beam-driven magnetic fluctuations are consistent with the model (figure 3(*b*)), but it would imply a nearly constant saturated fast particle content for any neutral beam current. The neutral particle analysis was localized in both radius and pitch-angle space. Using deuterium fuel in the NBI allows a calibrated measure of total fast

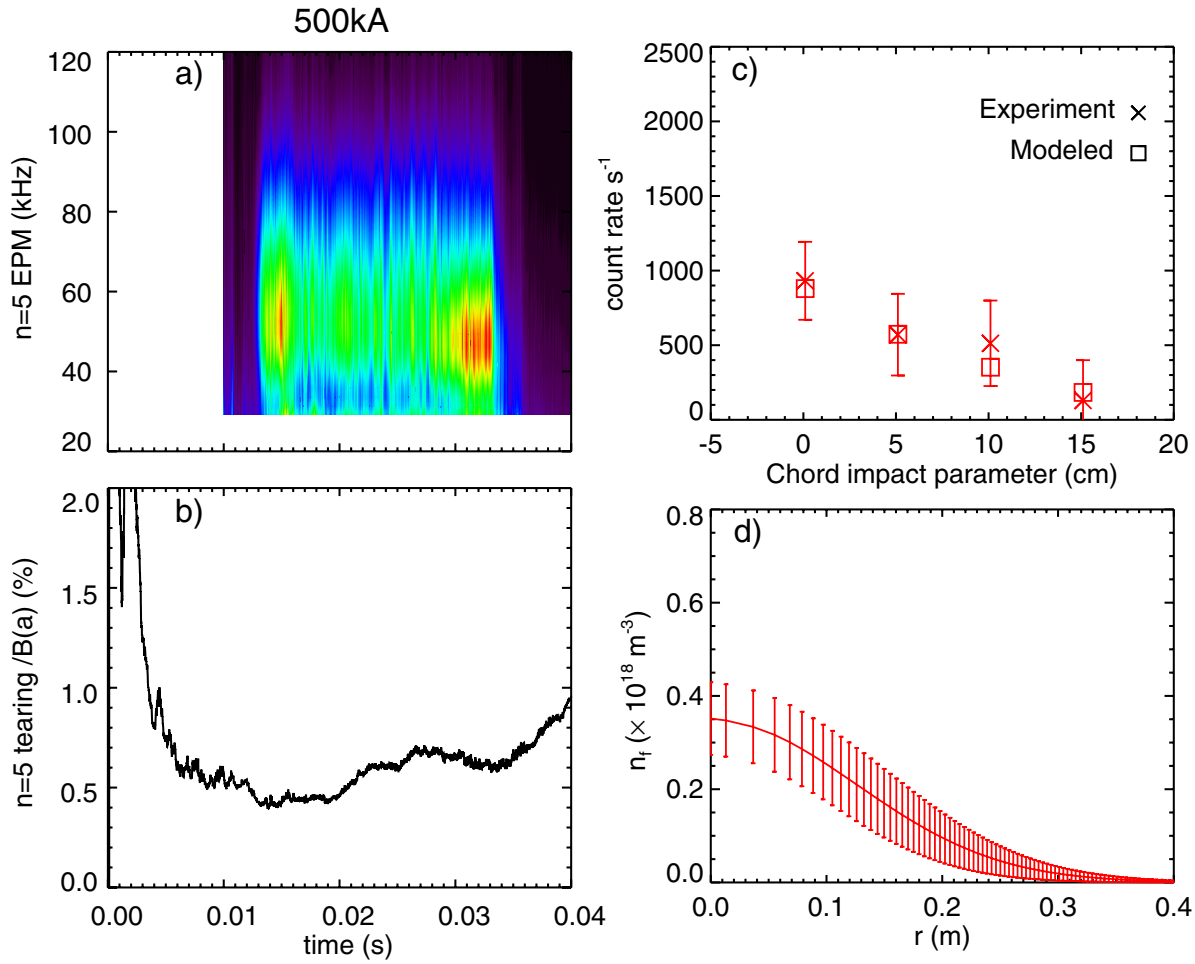

Figure 7. EPM (*a*) and tearing (*b*) activity during 25 kV D NBI into $I_p = 500$ kA discharges. When compared to the 300 kA case, it is clear the fast ion effect on tearing activity is reduced. The time-averaged fast ion density profile (*d*) is reconstructed from chord-integrated measurements (*c*) at $t = 30$ ms. Note that in contrast to the $I_p = 300$ kA case, the tearing mode does not settle into a stable value near the end of the NBI heating phase and this likely contributes to the relatively broader fast ion density profile.

ion content through fusion neutrons and exposes a key difference in fast ion content in the three cases.

The combination of EPM-induced re-distribution and tearing-driven transport together limit fast particle content, with a common denominator of each causing orbit stochasticity in different regions. The overlap of tearing mode-driven fast-ion islands effectively creates a location (near mid-radius) beyond which fast ions experience substantial radial guiding center velocity perturbations. Here they are diffusive and can be characterized by a finite confinement time [14]. In figure 8(*e*), the square symbol marks the diffusive boundary, radially defined by the innermost excursion of overlapping fast ion guiding center islands based on $\Delta q = q_{\rm fi} - q$ and tearing mode amplitudes. The fast particle density at the boundary is set by $\mathrm{d}N_f/\mathrm{d}t = S - N_f/\tau$ where S is the fast-ion source rate (proportional to NBI current) and a diffusive timescale τ is chosen to match a typical particle confinement time of 1 ms. A higher source rate would then set a larger n_f 'edge' value at this radius. The profile inward is then limited by critical gradient behavior due to bursting activity, similar to that observed in [30]. The spatial resolution of the fast ion density profile measurement is quite limited in this work, so for computing a fast ion density profile in this two-region model, a functional form for the EPM-limited critical gradient is specified. In recent work [31, 32] stability calculations are used to model critical gradients; toward the end of the works the computed critical gradient was mapped to parametric power law scaling in magnetic shear (s) and q. Critical gradients proportional to s/q^2 and s^2/q^2 are both found in the literature. We use a $\nabla n_{f,\rm crit} \propto s/q^2 = 6.4 \times 10^{17}\ \mathrm{m}^{-4}\ s/q^2$ where the single proportionality constant is chosen to match the experimental measurement in the full beam power ($I_{\rm beam} = 40$ A) case (in the $I_p = 300$ kA equilibrium). The RFP equilibrium has a monotonically rising s/q^2 profile that reaches a value $\sim$12 at the boundary between the EPM-limited region and tearing-limited region, giving a peak fast ion density gradient of about $7.5 \times 10^{18}\ \mathrm{m}^{-4}$, amusingly similar to the value of $\sim 8 \times 10^{18}\ \mathrm{m}^{-4}$ found for Alfvén eigenmode driven transport in DIII-D [33].

Integrating inward from the diffusive edge value yields lower values of $n_f(0)$ (and neutron flux) at lower beam current, consistent with the experiment. While the reduction in tearing mode amplitude is effectively the same in the $I_{\rm beam} = 40$ A and 30 A beam current cases, at $I_{\rm beam} = 20$ A this effect is nearly absent. The larger tearing mode amplitude at lower current increases the fast-ion island widths, pushing the diffusive

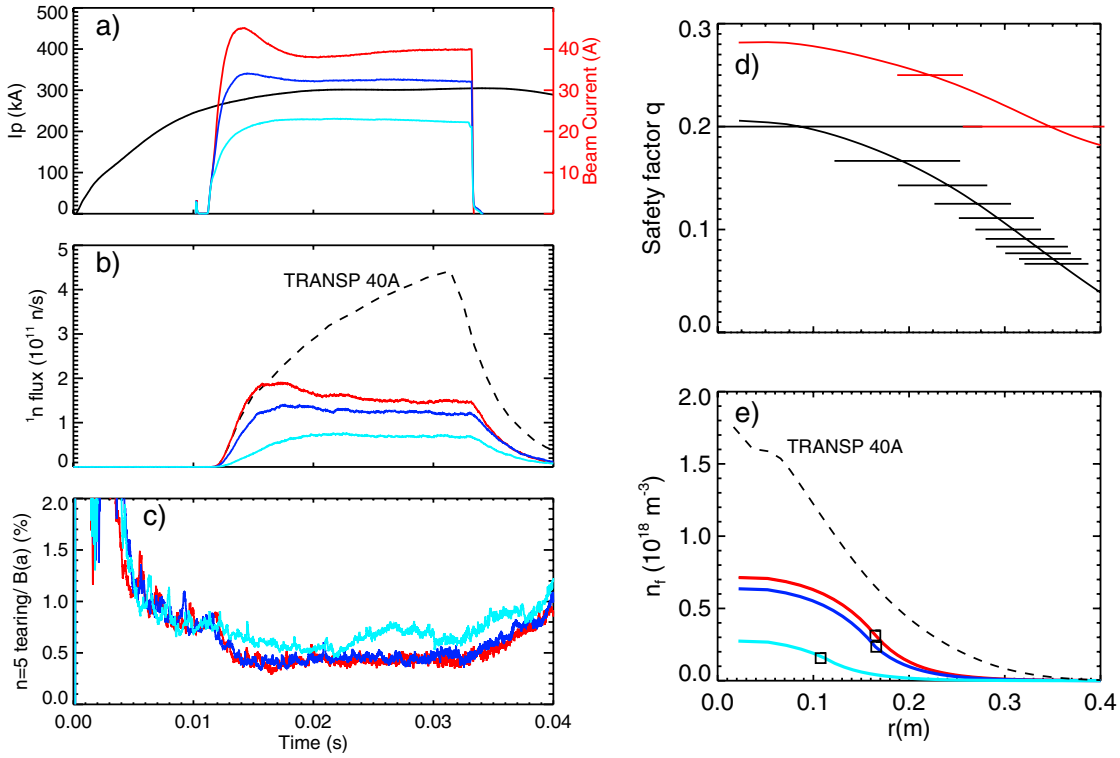

Figure 8. In $I_p = 300$ kA discharges, various neutral beam currents (a) result in different saturated levels of neutron flux (b). The ensembled $n = 5$ tearing mode activity (c) shows clear reduction for the two higher-beam current cases and a reduced effect at lowest beam current. q_{mag} (black) and q_f (red) with approximate island widths (d) set the diffusive boundary at which fast-ion islands overlap, shown as plot symbols on the two-region-model profiles in (e). The island widths plotted here correspond to the $I_{beam} = 40$ A case; the islands are nearly the same for $I_{beam} = 30$ A but are measurably wider for $I_{beam} = 20$ A. As discussed in the text, computation of the fast ion density profile by a model with a diffusive region outside this radius and a critical gradient-limited profile inside this radius leads to varied n_f profiles (e). The classical calculation for $I_{beam} = 40$ A (dashed line) predicts a much higher fast ion content. Calculations for (d) and (e) correspond to the $t = 30$ ms time slice.

boundary layer inward, leading to a further reduction in the fast-ion density at low beam current.

A crude test of this two-region model reveals it is imperfect. A profile-to-profile comparison is not justified, as the experimental data are inverted with a two-free parameter fit, while the model would require several parameters to match the shape following an s/q^2. Instead, an integration over the profile (including the velocity distribution for fusion reactivity) is compared to the experimentally saturated volume-integrated neutron flux. While the modeled total neutron flux is well-matched to the experimentally measured saturated value for the $I_{beam} = 40$ A (by choice of constant in the critical gradient), the model overestimates neutron flux for the $I_{beam} = 30$ A by ~10% and underestimates by ~25% for the $I_{beam} = 20$ A case. It does, however, illustrate the importance of tearing modes in development of the total fast ion population: this subtlety is not evident in beam-blip measurements of fast ion confinement time where Alfvénic activity is absent [13]. To illustrate the large discrepancy from classical transport only, the fast ion density profile from TRANSP is included in figure 8(e) for the $I_{beam} = 40$ A case.

When considering the 500 kA case (not plotted), the deviation of q_f from magnetic q is substantially reduced (figure 2(a)). This brings the radial location of the diffusive boundary closer to the plasma core. The relatively larger tearing amplitude reinforces this effect. Both contribute to an expected reduction in fast ion content relative to the 300 kA case, as observed.

6. Conclusion

A large population of fast ions rapidly builds in the core of the RFP during tangential NBI due to injection geometry. While they experience near-classical confinement times in the core, fast ions experience much poorer confinement near mid-radius where their orbits become stochastic and charge-exchange probabilities increase. A simple model that combines (1) a critical-gradient limited core population with (2) an outer-radius diffusive region and (3) a pedestal height set by particle source rate, explains the measured fast particle content over the explored experimental range.

The key result for Alfvénic stability in the RFP is at a modest $|B|(0) \sim 0.3$ T, where super-Alfvénic deuterium NBI ions at 25 kV substantially alter the equilibrium and tearing dynamics of the RFP discharge. The fast ion concentration ramps up (after a transient nonlinear state) to that of marginal stability to the EPM. Here we have identified a critical β_f gradient, beyond which the EPM efficiently moves particles to the regions of stochastic orbits. A central $\beta_f(0) = 7.55 \pm 0.48$ with volume-averaged $\langle\beta_f\rangle = 2.2 \pm 0.30$ is attained in a single equilibrium condition of $I_p = 300$ kA, after a classical slowing time of beam injection and with full beam power ($I_{beam} = 40$ A).

At higher plasma current and magnetic field strength, the 25 kV D + beam ions are sub-Alfvénic and only excite modest EPM activity. Confinement appears to be more

strongly influenced by the core tearing instability. The different behavior is due in part to a minimal departure of q_f from magnetic q in this case as well as small core tearing mode suppression from NBI. Only modest slowing or radial wandering will place the fast ion in a stochastic orbit where loss to the plasma boundary occurs rapidly.

The core-localized nature of the fast ion profiles leads to excitation of the EPM on the Alfvén continuum in a region of weakest magnetic shear in the natural RFP equilibrium fields. An experiment with substantially higher energy ions and off-axis injection (currently out of experimental reach) would prod different regions of magnetic shear and possible continuum gaps.

Acknowledgments

This material is based upon work supported by the U.S. Department of Energy Office of Science, Office of Fusion Energy Sciences program under Award Number DE-FC02-05ER54814. Portions of the work were accomplished with the use of infrastructure of Complex DOL (BINP, Russia).

References

[1] Heidbrink W.W. and Sadler G. 1994 *Nucl. Fusion* **34** 535–615
[2] Zonca F. and Chen L. 2000 *Phys. Plasmas* **7** 4600–8
[3] Fu G.Y. and van Dam J.W. 1989 *Phys. Plasmas* **1** 1949–52
[4] Chen L. 1994 *Phys. Plasmas* **1** 1519
[5] Strait E.J., Heidbrink W.W., Turnbull A.D., Chu M.S. and Duong H.H. 1993 *Nucl. Fusion* **33** 1849–70
[6] Heidbrink W.W., Strait E.J., Doyle E., Sager G. and Snider R.T. 1991 *Nucl. Fusion* **31** 1635–48
[7] Heidbrink W.W., Strait E.J., Chu M.S. and Turnbull A.D. 1993 *Phys. Rev. Lett.* **71** 855–8
[8] Heidbrink W. 1995 *Plasma Phys. Control. Fusion* **37** 937–49
[9] Kramer G.J., Tobias B.J., Nazikian R., Holcomb C., Collins C.S., van Zeeland M.A., Heidbrink W.W. and Zhu Y. 2016 Suppressing Alfvén eigenmodes by q-profile engineering to improve fast-ion confinement *APS Meeting Abstracts (San Jose, CA, 31 October–4 November 2016)* JP10.126 (http://meetings.aps.org/Meeting/DPP2016)
[10] Biewer T.M., Forest C.B., Anderson J.K., Fiksel G., Hudson B., Prager S.C., Sarff J.S. and Wright J.C. 2003 *Phys. Rev. Lett.* **91** 045004
[11] Heidbrink W.W., Kim J. and Groebner R.J. 1988 *Nucl. Fusion* **28** 1897–901
[12] Heidbrink W.W. and Sager G. 1990 *Nucl. Fusion* **30** 1015–25
[13] Fiksel G., Hudson B.F., Den Hartog D.J., Magee R.M., O'Connell R., Prager S.C., Beklemishev A.D., Davydenko V.I., Ivanov A.A. and Tsidulko Y.A. 2005 *Phys. Rev. Lett.* **95** 125001
[14] Hudson B.F. 2006 Fast ion confinement in the reversed-field pinch *PhD Thesis* University of Wisconsin
[15] Anderson J.K., Capecchi W.J., Eilerman S., Koliner J.J., Nornberg M.D., Reusch J.A., Sarff J.S. and Lin L. 2014 *Plasma Phys. Control. Fusion* **56** 094006
[16] Bonofiglo P.J., Anderson J.K., Boguski J., Kim J., Egedal J., Gobbin M., Spong D.A. and Parke E. 2019 *Phys. Plasmas* **26** 022502
[17] Dexter R.N., Kerst D.W., Lovell T.W., Prager S.C. and Sprott J.C. 1991 *Fusion Technol.* **19** 131–9
[18] Anderson J.K. *et al* 2013 *Phys. Plasmas* **20** 056102
[19] Koliner J.J. 2012 *Phys. Rev. Lett.* **109** 115003
[20] Lin L. *et al* 2014 *Phys. Plasmas* **21** 056104
[21] 2008 *FESAC Toroidal Alternates Panel Final Report* (http://fusion.gat.com/tap/final_report.php)
[22] Goldston R., McCune D., Towner H., Davis S., Hawryluk R. and Schmidt G. 1981 *J. Comput. Phys.* **43** 61–78
[23] Liu D. *et al* 2011 *38th EPS Conf. on Plasma Physics (Strasbourg, France, 27 June–1 July 2011)* pp 3–6 (http://ocs.ciemat.es/EPS2011PAP/html/)
[24] Eilerman S., Anderson J.K., Reusch J.A., Liu D., Fiksel G., Polosatkin S. and Belykh V. 2012 *Rev. Sci. Instrum.* **83** 10D302
[25] Capecchi W. 2017 A critical fast ion beta in the Madison Symmetric Torus reversed field pinch *PhD Thesis* University of Wisconsin
[26] Capecchi W., Anderson J., Bonofiglo P., Kim J. and Sears S. 2016 *Rev. Sci. Instrum.* **87** 11D826
[27] Magee R., Anderson J.K., Korepanov S., Frausto L., Boguski J., Bonofiglo P.J., Kim J. and McConnell R. 2018 *Rev. Sci. Instrum.* **89** 10I104
[28] Parke E. 2014 Diagnosis of internal structures in a RFP using electron temperature fluctuations *PhD Thesis* University of Wisconsin
[29] Lin L. *et al* 2013 *Phys. Plasmas* **20** 030701
[30] Collins C.S., Heidbrink W.W., Austin M.E., Kramer G.J., Pace D.C., Petty C.C., Stagner L., Van Zeeland M.A., White R.B., Zhu Y.B. and (DIII-D Team) 2016 *Phys. Rev. Lett.* **116** 095001
[31] Waltz R.E., Bass E.M., Heidbrink W.W. and van Zeeland M.A. 2015 *Nucl. Fusion* **55** 123012
[32] Sheng H., Waltz R.E. and Staebler G.M. 2017 *Phys. Plasmas* **24** 072305
[33] Collins C.S., Heidbrink W.W., Podestà M., White R.B., Kramer G.J., Pace D.C., Petty C.C., Stagner L., van Zeeland M.A. and Zhu Y.B. 2017 *Nucl. Fusion* **57** 086005